INSTITUTE OF PHYSICS PUBLISHING and INTERNATIONAL ATOMIC ENERGY AGENCY NUCLEAR FUSION

Nucl. Fusion **44** (2004) 560–570 PII: S0029-5515(04)77329-9

The resistive wall mode and feedback control physics design in NSTX

S.A. Sabbagh[1], J.M. Bialek[1], R.E. Bell[2], A.H. Glasser[3], B.P. LeBlanc[2], J.E. Menard[2], F. Paoletti[1], M.G. Bell[2], R. Fitzpatrick[4], E.D. Fredrickson[2], A.M. Garofalo[1], D.A. Gates[2], S.M. Kaye[2], L.L. Lao[5], R. Maingi[6], D. Mueller[2], G.A. Navratil[1], D. Stutman[7], W. Zhu[1] and the NSTX Research Team

[1] Department of Applied Physics and Applied Mathematics, Columbia University, New York, NY, USA
[2] Princeton Plasma Physics Laboratory, Princeton University, Princeton, NJ, USA
[3] Los Alamos National Laboratory, Los Alamos, NM, USA
[4] University of Texas at Austin, Austin, TX, USA
[5] General Atomics, San Diego, CA, USA
[6] Oak Ridge National Laboratory, Oak Ridge, TN, USA
[7] Johns Hopkins University, Baltimore, MD, USA

E-mail: sabbagh@pppl.gov

Received 18 March 2003, accepted for publication 16 February 2004
Published 30 March 2004
Online at stacks.iop.org/NF/44/560
DOI: 10.1088/0029-5515/44/4/011

Abstract
One of the goals of the National Spherical Torus Experiment (NSTX) is to investigate the physics of global mode stabilization in a low aspect ratio device. NSTX has a major radius $R_0 = 0.86$ m, a midplane half-width of 0.7 m, and an on-axis vacuum toroidal field $B_0 \leqslant 0.6$ T and has reached a plasma current $I_p = 1.5$ MA. Experiments have established the wall-stabilized MHD operating space of the machine. The maximum β_t and β_N have reached 35% and 6.5%, respectively, with β_N reaching $9.5l_i$. Collapses in plasma toroidal rotation and β_t have been correlated with violation of the $n = 1$ ideal MHD beta limit, $\beta_{N\,\text{no-wall}}$, computed by the DCON stability code using time-evolving EFIT reconstructions of experimental discharges. The resistive wall mode (RWM) was observed over a wide range of β_N when $\beta_{N\,\text{no-wall}}$ was exceeded. Plasma toroidal rotation damping during the RWM was rapid and global. Damping rates were more than five times larger than caused by low toroidal mode number rotating modes alone, which displayed a slower, diffusive rotation damping away from the rational surface. The rotation damping rate and dynamics depend on the applied toroidal field and the computed minimum value of the safety factor. The computed RWM perturbed field structure from experimental plasma reconstructions has been input to the VALEN feedback analysis code for quantitative comparison of experimental and theoretical RWM growth rates and to analyse the effectiveness of various active feedback stabilization designs. The computed RWM $n = 1$ mode growth rate, which depends on plasma equilibrium parameters such as β_N and pressure profile peaking, agrees well with experimental growth rates in different operating regimes. Increasing β_N in the ST initially improves mode coupling to the stabilizing wall; however, at the highest β_N values reached, the ideal with-wall beta limit, $\beta_{N\,\text{wall}}$, is approached, the effectiveness of the passive stabilizing plates is reduced, and the computed RWM growth rate approaches ideal MHD growth rates. Several active mode control designs were considered and evaluated. The most effective configuration is computed to provide stabilization at β_N up to 94% of the ideal with-wall limit.

PACS numbers: 52.55.Fa, 52.55.Tn, 52.65.Kj, 52.35.Py

(Some figures in this article are in colour only in the electronic version)

1. Introduction

Efficient fusion reactor designs maximize the ratio of the confined plasma energy to the applied magnetic field. The low aspect ratio spherical torus (ST) design [1–3] utilizes favourable magnetic field geometry to improve plasma stability with a reduced toroidal field. Further increases in $\beta_t \equiv 2\mu_0\langle p\rangle/B_0^2$ and $\beta_N \equiv 10^8\langle\beta_t\rangle a B_0/I_p$ are possible with equilibrium profile and boundary shape optimization and passive/active control of global instabilities. Experiments

to date have shown that the ideal MHD stability limit sets the maximum stable operating beta for advanced tokamak plasmas. Devices with a stabilizing conducting structure generally have the highest beta limits, defined as the 'with-wall' limit, $\beta_{\mathrm{N\,wall}}$, for a given toroidal mode number and wall configuration. At this value, internal pressure and current driven kink/ballooning instabilities set the β limit. A similar 'no-wall' limit, $\beta_{\mathrm{N\,no\text{-}wall}}$, occurs in devices without a passive stabilizing conducting structure. In this case, plasmas are subject to global modes with increased amplitude at the plasma/vacuum boundary that become unstable at $\beta_{\mathrm{N\,no\text{-}wall}} < \beta_{\mathrm{N}} < \beta_{\mathrm{N\,wall}}$. In addition, if the plasma rotation is sufficiently low in a device with a stabilizing conducting structure, the beta limit can be reduced from $\beta_{\mathrm{N\,wall}}$ to $\beta_{\mathrm{N\,no\text{-}wall}}$ by the destabilization of resistive wall modes (RWMs). In such a case, the RWM might be stabilized by active means [4]. Active mode control is expected to be important for fusion reactors since plasmas in these devices may not have sufficient rotation speed to rely upon passive stabilization alone. Similarities between the advanced tokamak and the ST lead one to expect that stabilization of the ST plasma would follow the tokamak experience. Generally, this appears to be correct; however, the dependence of the stability limit on equilibrium profiles, the role of an elevated safety factor, the alteration of global mode structure, and the magnitude and physical mechanism of plasma rotation damping due to instabilities are examples of stability physics that must be evaluated specifically for ST plasmas. Experimental verification and theoretical understanding of these physics elements are required input for a practical design of a global instability control system for the ST. Of particular importance in maximizing passive stabilization in such a system is understanding the physical mechanisms that decrease the plasma toroidal rotation most severely. In section 2, the operation of passively stabilized plasmas with β_{N} greater than $\beta_{\mathrm{N\,no\text{-}wall}}$ is shown, and the dependence of the maximum β_{N} achieved as a function of current and pressure profile parameters is examined. Section 3 describes the RWM, rotation damping, and β evolution while operating at high β_{N} in excess of $\beta_{\mathrm{N\,no\text{-}wall}}$. The stabilizing capability of the present National Spherical Torus Experiment (NSTX) conducting structure is examined, and a physics design of an active stabilization system is given in section 4. Beta-limiting MHD instabilities in recent NSTX plasmas are discussed more generally in [5]. In this paper, we concentrate on ideal MHD stability limits and the RWM. A comparison is made between RWMs at a relatively low β_{N} and relatively high static error field and RWM dynamics in high β_{N} H-mode plasmas with a reduced error field. Throughout this paper, the ideal no-wall and with-wall beta limits are computed using the DCON code [6]. A summary and conclusions are given in section 5.

2. Wall-stabilized operating space

The design of the NSTX enables investigation of the physics of global MHD mode stabilization at low aspect ratios. The device has a major radius $R_0 = 0.86$ m, a midplane half-width of 0.7 m, and an on-axis vacuum toroidal field $B_0 \leqslant 0.6$ T, and has operated at a plasma current $I_{\mathrm{p}} = 1.5$ MA. Figure 1 illustrates the device, highlighting the passive stabilizing plates. The stabilizers are arranged as four toroidal rings of 48 independent copper plates covered by graphite tiles. The plates are electrically connected indirectly through the vacuum vessel since each is attached to it by high resistance mounts. Auxiliary heating and current drive systems include up to 7 MW of neutral beam heating and up to 6 MW of high-harmonic fast wave power. The MHD instability diagnostics include poloidal and toroidal arrays of magnetic pickup coils, six midplane mounted saddle loops instrumented to measure toroidal mode number $n = 1$ locked modes, and horizontal and vertical arrays of ultra soft x-ray detectors. Plasma toroidal rotation profiles are measured by a 16 channel charge exchange recombination spectroscopy system with 20 ms time resolution.

High beta operation with equilibria reaching the ideal 'no-wall' MHD stability limit ($\beta_{\mathrm{t}} = 25\%$, $\beta_{\mathrm{N}} = 4.3$) was previously reported, and a path towards wall-stabilized, high beta operation was described (see figure 14 of [7]). Limitation of β_{N} to the ideal no-wall limit (at a maximum of $6l_{\mathrm{i}}$), where l_{i} is the plasma internal inductance, indicated that the passive stabilizer plates in the device had minimal effect on gross plasma instabilities. However, in recent experiments, plasmas have exceeded significantly the ideal no-wall limit and have reached $\beta_{\mathrm{N}}/\beta_{\mathrm{N\,no\text{-}wall}} = 1.35$ in plasmas reaching the maximum β_{N} in the device. The present wall-stabilized operating space is shown in figure 2. Present maximum beta values are $\beta_{\mathrm{t}} = 35\%$ and $\beta_{\mathrm{N}} = 6.5$. The poloidal beta, β_{p}, has reached 1.5. The ratio $\beta_{\mathrm{N}}/l_{\mathrm{i}}$ has reached 9.5, and wall stabilization has eliminated the constraint expected by advanced tokamak empirical beta limit scalings in which $\beta_{\mathrm{N}}/l_{\mathrm{i}}$ is constant [8]. This result is of particular importance to the success of the ST as a fusion device since operation at both high β_{N} and low l_{i} are necessary to maximize bootstrap current profile alignment as well as magnitude. These characteristics minimize current drive requirements and recirculating power in reactor designs. The previously observed trend of maximum β_{N} increasing with decreasing pressure profile peakedness, F_{p}, defined as the ratio of peak to volume-averaged pressure, remains true for wall-stabilized plasmas (figure 3). Operation at reduced F_{p} in present experiments has been made possible by routine H-mode operation [9]. Global plasma parameters quoted in this paper, including F_{p}, are reconstructed with the EFIT code [10] using partial kinetic pressure profile information and the measured plasma diamagnetism [7].

Recent expansion to increased β_{N} is related to three key operational and device improvements. First, the static error field in the machine has been reduced significantly by realignment of the upper main equilibrium field coil. This improvement has reduced the $n = 1$ static error field by greater than an order of magnitude and is now calculated as less than 0.5 G at R_0 and less than 2 G at the outer limiter at the midplane [5]. This is expected to reduce the negative impact of tearing modes and RWMs on plasma performance and longevity. Second, H-mode operation has created plasmas with pressure peaking factors below 1.9. Ideal MHD stability calculations show that broader pressure profiles yield global modes that are more external and therefore amenable to stabilization by the passive stabilizer plates. Third, both magnetics-only and partial kinetic EFIT reconstructions indicate that the minimum q value, q_{min}, in long pulse, high β_{N} plasmas is maintained

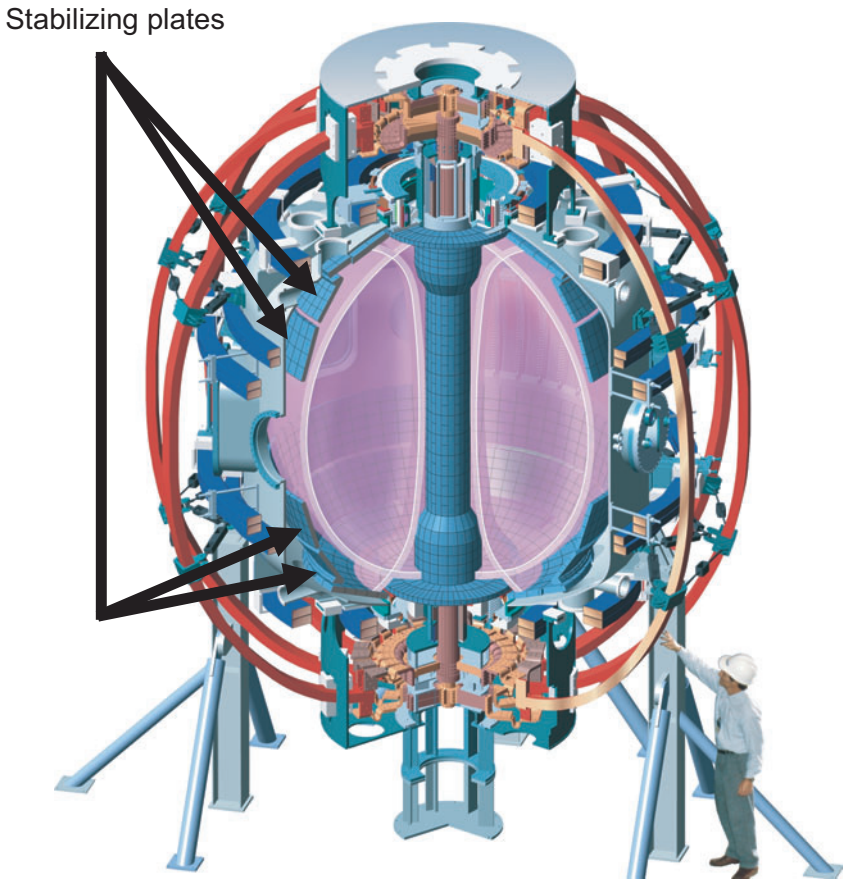

Figure 1. Illustration of NSTX, highlighting the passive stabilizing conducting plates.

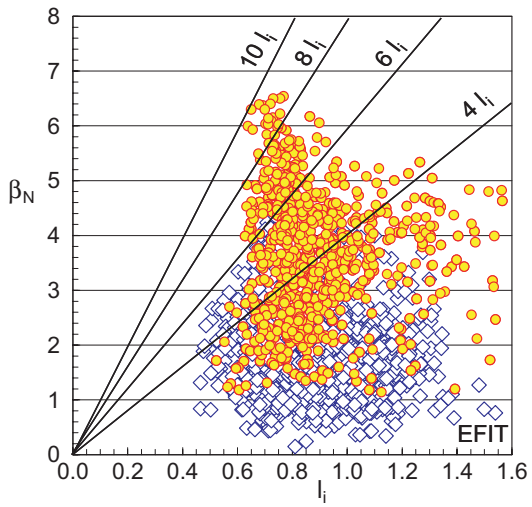

Figure 2. Normalized beta versus plasma internal inductance. Recent NSTX plasmas (shaded circles) have exceeded the CY01 nominal 'no-wall' beta limit of $6l_i$.

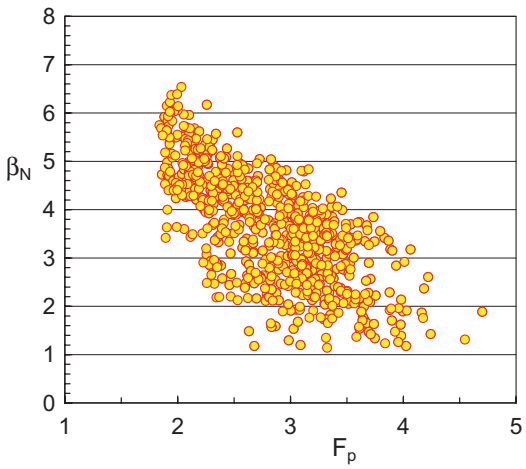

Figure 3. Normalized beta versus pressure peaking factor.

above unity and increases with time to values greater than 2. Note that internal magnetics data were not available for these reconstructions. The results of these alterations are illustrated in figure 4. In figure 4(a), the plasma created with a high static error field suffers a terminating β collapse at $\beta_N = 2.8$ and $F_p = 3.4$ after the onset of a RWM. The computed $n = 1$ ideal $\beta_{N\,\text{no-wall}}$ is 2.6. In figure 4(b), a recent plasma with similar β_N and F_p suffers a similar β collapse initially. However, there is no observed mode locking, and β_N recovers. As the previous peak β_N is reached, the plasma transitions to H-mode, reducing F_p, increasing $\beta_{N\,\text{no-wall}}$, and allowing the plasma to access higher β_N. In the latter case, $q_{\min} > 1$ is maintained initially at a low poloidal beta by an increase in the vacuum field to $B_0 > 0.4$ T. As the poloidal beta increases, TRANSP calculations show a significant bootstrap current fraction up

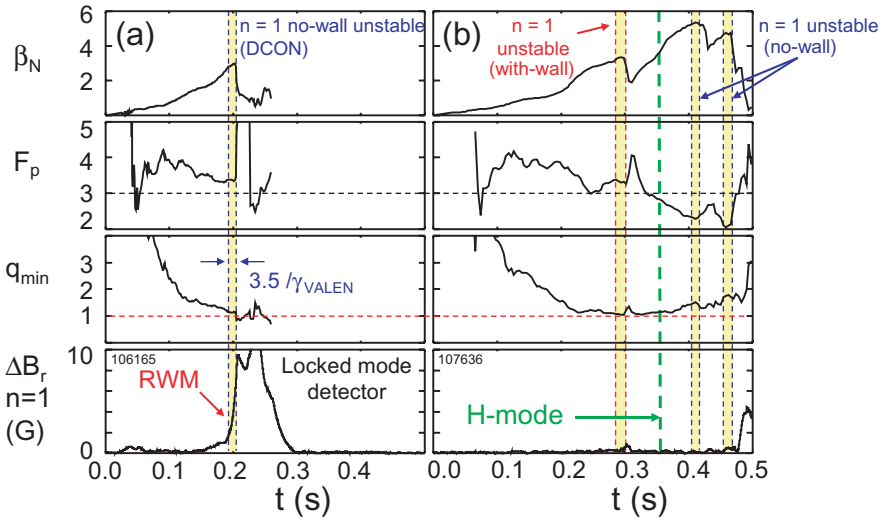

Figure 4. Time evolution of β_N, pressure peaking factor, q_{min}, and $n = 1$ LMD signal for (a) an L-mode plasma with relatively high $n = 1$ static error field and (b) for a recent plasma with $n = 1$ static error field reduced by an order of magnitude and transitioning to H-mode after recovery from the initial beta collapse.

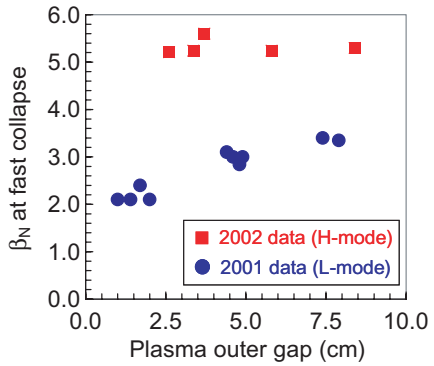

Figure 5. Dependence of observed β_N at the time of a fast collapse versus plasma outer gap for L-mode plasmas at a relative high static error field (●) and H-mode plasmas with a reduced error field (■).

to 50% and a total non-inductive current of 60%, which are believed to cause the observed saturation, or reduction in l_i, and corresponding increase in q_{min}. The importance of the increased q_{min} in sustaining the stabilization of plasmas above the ideal no-wall beta limit is discussed in section 3.

Another result of recent high β_N H-mode operation is that the observed β_N limit is insensitive to the proximity of the plasma to the stabilizing plates. Figure 5 shows a comparison of experimental results taken before/after the alteration of the static error field and without/with H-mode operation, for which the proximity to the passive stabilizer plates was varied. The gap between the plasma and the outer limiter is measured on the outboard midplane. The earlier L-mode plasmas show a decrease in the peak β_N reached before the β collapse as the plasma outer gap decreases. This trend is expected theoretically for the RWM, which becomes less stable as the outer gap decreases [11]. An alternate and perhaps equivalent hypothesis for this behaviour is that the static error field is computed to increase at a larger major radius, possibly leading to a reduced β_N limit as the outer gap is reduced [12]. In contrast, the H-mode plasmas at higher β_N show no variation in the peak β_N reached as a function of the plasma outer gap. This is consistent with ideal MHD calculations for these low aspect ratio equilibria since at $\beta_N \sim 5$, low-n global modes couple well with the passive stabilizing structure, regardless of the plasma outer gap in the range tested [7]. The lack of a reduction in the peak β_N as the gap is reduced may be due to the reduction in the static error field.

3. RWMs at high normalized beta

For a given plasma equilibrium, stable operation at maximum plasma beta theoretically occurs when external kink/ballooning modes are stabilized by a perfectly conducting wall sufficiently close to the plasma boundary (the ideal with-wall beta limit). However, it has been shown both theoretically [11, 13] and experimentally [14, 15] that realistic segmented and resistive conducting walls used for plasma stabilization allow for the destabilization of the RWM when the plasma beta exceeds $\beta_{N\,no\text{-}wall}$. The RWM is a global kink/ballooning plasma mode that is rotating sufficiently slowly ($\Omega \sim 1/\tau_{wall}$), so that the perturbed field can penetrate the stabilizing conducting structure. Stabilization of the RWM is possible but requires a rotation rate of order $(k_\parallel a)V_A$, where $k_\parallel$ is the parallel wave number, a is the plasma minor radius, and V_A is the Alfvén speed [16]. This critical rotation frequency, Ω_c, for RWM stabilization has been observed in advanced tokamak experiments [15], and because of the low $k_\parallel$ of the mode is a few per cent of the Alfvén frequency at the $q = 2$ surface. Similar values are computed for plasmas exhibiting RWMs in NSTX. The RWM typically leads to rotation damping and subsequent β collapse and plasma termination in advanced tokamaks. However, since the mode grows slowly ($\gamma \sim 1/\tau_{wall}$), active feedback stabilization is feasible in plasmas with toroidal rotation insufficient for passive stabilization.

While the general concept of the RWM applies to both the advanced tokamak and ST, it is important to study the differences in the mode physics at low aspect ratios. For example, the mode geometry is altered significantly in the ST,

leading to differences in coupling of the mode to the wall, especially at extremes in β_N. In NSTX, the $n = 1$ RWM was observed initially when the ideal no-wall β_N limit was violated in experiments aimed at maximizing coupling of the plasma to the stabilizing conducting plates [7]. The plasmas were limited and did not transition to H-mode. This yielded a relatively high $F_p = 3.4$, and therefore low $\beta_{N\,\text{no-wall}} \sim 2.6$, and only a small difference between no-wall and with-wall β_N limits, $\Delta\beta_N = \beta_{N\,\text{wall}} - \beta_{N\,\text{no-wall}} = 0.2$. At this low level of β_N, coupling of the mode eigenfunction to the wall can be weak, and so the plasma–wall gap was kept small, approximately 15% of the plasma minor radius, to maximize coupling. These experiments were also conducted before the $n = 1$ static error field was reduced. Primary diagnostics used to detect the instability were the $n = 1$ locked mode detector (LMD), and the plasma toroidal rotation measured by charge exchange recombination spectroscopy. The mode was not observed when $\beta_N < \beta_{N\,\text{no-wall}}$ as computed by time-evolving ideal MHD stability calculations using DCON [6]. RWMs in plasmas with $\beta_{N\,\text{no-wall}} \sim 2.6$ either exhibited the RWM or neoclassical tearing modes but not both. The RWM was observed on the LMD while the plasma stored energy increased. This observation occurred while the plasma was rotating, eliminating the possibility that the mode was a locked tearing mode. No precursors were observed with the magnetic pickup coils, and no core or edge islands were observed before the onset of the RWM. Ultra-soft x-ray emission preceding the beta collapse indicated a kinking of the plasma core. In the comparison plasma with $\beta_N < \beta_{N\,\text{no-wall}}$, clear $n = 2$ and $n = 3$ rotating modes were detected before the beta saturation and ultra-soft x-ray emission showed a radially symmetric reconnection event leading to the termination, rather than a kink. RWMs observed with a high static error field generated an $n = 1$ field perturbation of $\sim$7 G in the LMD at the time of the beta collapse that led to plasma termination. The VALEN computed $n = 1$ inverse mode growth rate, or mode growth time, $1/\gamma_{\text{VALEN}}$ of 4.6 ms (see section 4 for details), agrees well with the experimental RWM growth time of 5 ms from the LMD signal. Based on this calculation, the experimental RWM persisted for $3.5/\gamma_{\text{VALEN}}$ before termination at the beta collapse (figure 4(*a*)).

Recently, the RWM has been studied with a reduced static error field in H-mode plasmas with significantly lower $F_p \sim 2$, higher $\beta_N > 6$, and larger $\Delta\beta_N = 2$. Under these conditions, it is now rare to find pure RWM activity separate from tearing mode activity. This observation might be due in part to an increased difficulty in measuring the RWM field perturbation with the present LMD at the reduced static error field. LMD signals of between 0.6 and 1.0 G are now more typical during the RWM. The RWM growth time computed by VALEN is 20 ms, in agreement with the growth rate of the LMD signal. This is four times longer than the RWM growth time measured in and computed for L-mode plasmas with greater pressure profile peakedness; however, the normalized period over which the no-wall beta limit is violated remains the same in both cases at $\Delta t = 3.5/\gamma_{\text{VALEN}}$ for the $n = 1$ mode. A common feature of RWMs at high and low β_N is the strong toroidal rotation damping observed in both, in spite of increased neutral beam momentum input over lower beta plasmas. The magnitude of the rotation damping, as well as the detail of the rotation profile

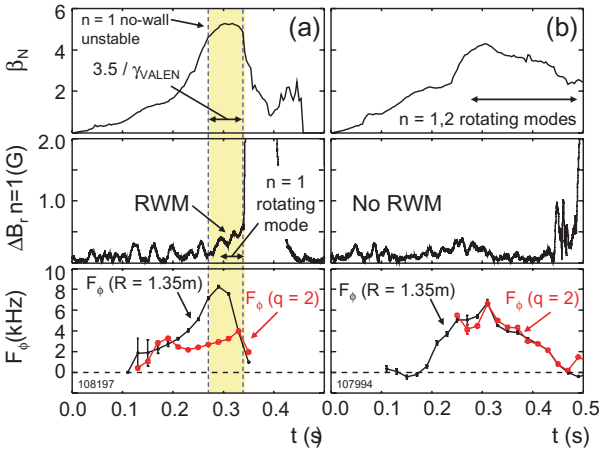

Figure 6. Time evolution of β_N, $n = 1$ LMD signal and toroidal plasma rotation at $R = 1.35$ m and the outboard major radial position of the computed $q = 2$ surface for a plasma with $\beta_N > \beta_{N\,\text{no-wall}}$ exhibiting a RWM (frame (*a*)) and $\beta_N < \beta_{N\,\text{no-wall}}$ exhibiting rotating plasma modes alone (frame (*b*)).

dynamics, distinguishes the RWM from tearing mode activity and suggests a very different physical mechanism for rotation damping between the two modes. Figure 6 shows the evolution of a plasma with β_N exceeding $\beta_{N\,\text{no-wall}}$, compared with a plasma that does not. In the former case, the observed RWM shows only a weak signal in the LMD and is accompanied by $n = 1$ rotating mode activity as the RWM grows. The LMD signal reaches just 0.6 G before the accompanying $n = 1$ rotating mode locks. The rotation damping rate near $q = 2$ is $-174\,\text{kHz}\,\text{s}^{-1}$. In contrast, plasmas exhibiting rotating modes alone exhibit relatively weak rotation damping. Figure 6(*b*) illustrates the evolution of a similar plasma with $\beta_N < \beta_{N\,\text{no-wall}}$ initially exhibiting $n = 1$ and 2 rotating mode activity, with $n = 2$ largely damped approximately 60 ms after the mode onset. Magnetic pickup coils show $n = 1$ oscillations with a frequency slowly decreasing from 8 kHz, consistent with the observed toroidal rotation frequency, F_ϕ, decrease in the region of the EFIT computed $q = 2$ surface. The rotation damping rate at $q = 2$ is nearly constant at $-29\,\text{kHz}\,\text{s}^{-1}$, more than five times less rapid than in the plasma with $\beta_N > \beta_{N\,\text{no-wall}}$. The evolution of the plasma toroidal rotation profiles for the plasmas shown in figure 6 is shown in figure 7. In the plasma with $\beta_N > \beta_{N\,\text{no-wall}}$ (frame (*a*)), toroidal rotation damping occurs across most of the plasma cross-section simultaneously. The process appears non-diffusive and similar to the rotation damping process observed from error field induced locked modes when field penetration occurs [17, 18]. In contrast, when $\beta_N < \beta_{N\,\text{no-wall}}$ (frame (*b*)), the profile dynamics show the damping to be diffusive, with a flattening of the rotation profile originating just inside the $q = 2$ surface and penetrating slowly to the plasma core. Mode locking eventually occurs 0.2 s later, when rotation at $q = 2$ drops to the critical value for electromagnetic torque induced magnetic island locking of approximately half the initial value, $\omega_0/2$. This process is in agreement with the theory of rotation damping due to a magnetic island in the presence of a conducting wall [19]. The RWM therefore greatly reduces the time it normally takes the island to reach $\omega_0/2$.

Another remarkable detail of the rotation damping process is that the edge rotation remains essentially unchanged during

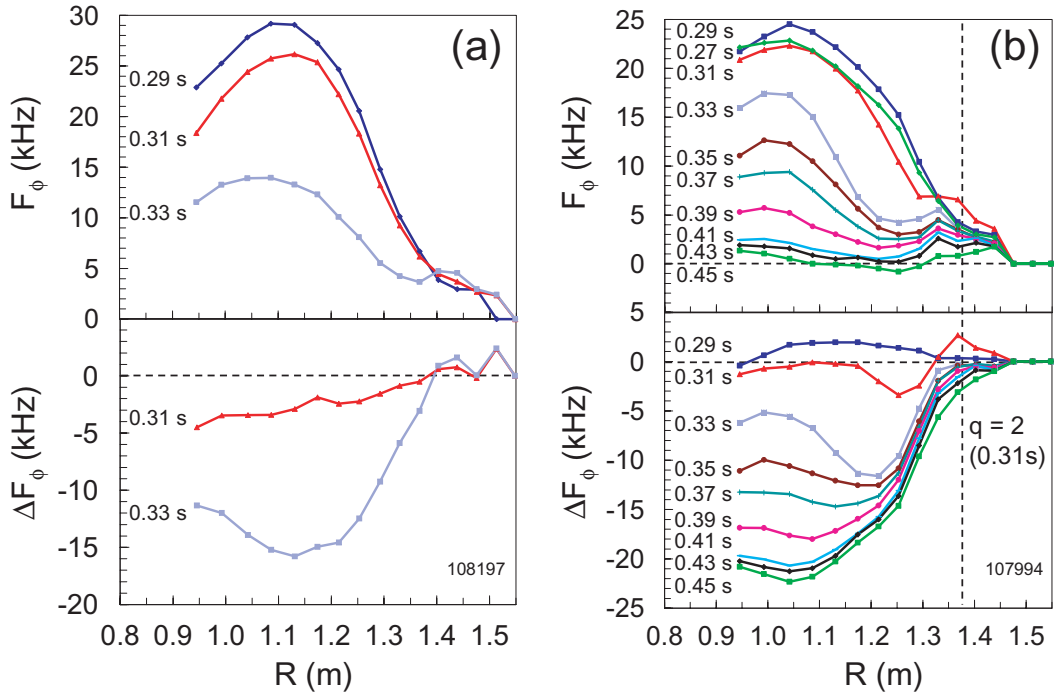

Figure 7. Toroidal rotation profile dynamics for an H-mode plasma with $\beta_N > \beta_{N\,\text{no-wall}}$ exhibiting a RWM (frame (*a*)) and $\beta_N < \beta_{N\,\text{no-wall}}$ exhibiting rotating plasma modes alone (frame (*b*)).

RWM induced rotation damping, whereas the case of slow rotation damping due to islands shows a viscous drag outside $q = 2$ for longer times. This can be explained qualitatively by invoking a model of neoclassical viscous drag [20, 21] in the nearly static magnetic field perturbation of the RWM. This model has been used successfully to describe error field induced locked mode damping in JET and DIII-D [17, 18]. By this physics, local rotation damping scales as $\delta B_r^2 T_i^{0.5}$, where δB_r is the local perturbed field and T_i is the ion temperature. Therefore, it is expected that the rotation damping would be greatly reduced in the colder outer region of the plasma, consistent with the observation. This mechanism is non-resonant and consistent with the global, rather than local, nature of the observed plasma rotation damping. Profiles of electron temperature from a 20 channel Thomson scattering diagnostic (shown in figure 8) illustrate the plasma displacement during the growth of the RWM and at nearly constant plasma stored energy. By the time of the second profile, time-evolved stability analysis from the DCON code shows the plasma to be unstable to an $n = 1$ ideal kink/ballooning mode. The displacement appears as a global, asymmetric shift of the electron temperature profile. The full calculation of the theoretical drag profile due to neoclassical toroidal viscosity and quantitative comparison with experimental results is outside the scope of this work. However, an estimate of the drag magnitude and profile can be made using an estimate of the δB magnitude from $\delta B/B_0 \sim \delta r_{T_e}/a$, where δr_{T_e} is the measured T_e displacement, and the profile using a global eigenfunction form. This estimate reproduces the measured rotation damping profile shape and agrees quantitatively with experimental findings within a factor of 1.5. The measured displacement was reproduced in several repeated discharges and was only observed when β_N exceeded the no-wall beta limit. At this time, continuous low frequency rotating modes are absent from the plasma (figure 9). At $t = 0.32$ s, a burst of broadband MHD activity occurs, followed by a pure $n = 2$ rotating mode at 35 kHz. The sudden onset of this mode, with a broadband precursor, suggests that the $n = 2$ mode may have been triggered by the RWM displacement inducing a forced reconnection due to flux compression.

Long pulse ST plasma operation surpassing the current relaxation time, τ_{cr}, with $\beta_N > \beta_{N\,\text{no-wall}}$ is a goal of NSTX [22]. Since sufficient plasma rotation is required to stabilize low-n kink/ballooning modes, the rapid rotation damping associated with RWM destabilization appears to be a major impediment to reaching this goal since it curtails the high β_N period to $3.5\tau_{wall} \ll \tau_{cr}$. However, present results have already shown significant progress by maintaining $\beta_N > \beta_{N\,\text{no-wall}}$ for much longer periods. A key to this success has been operation with an increased applied toroidal field. Figure 10 shows the evolution of the toroidal rotation frequency in the core of the plasma for similar discharges with the same $I_p = 0.8$ MA but with several values of B_0. Also shown is the EFIT computed q_{min} for each plasma at peak β_N. RWMs are observed in the discharges with $B_0 = 0.34$ T ($q_{min} = 1.4$) and $B_0 = 0.39$ T ($q_{min} = 1.7$), leading to rapid core rotation damping. However, as B_0 is raised to 0.44 T ($q_{min} = 1.9$), the $n = 1$ signature of the RWM is no longer apparent in the LMD signal, the rotation damping significantly decreases, and the pulse length is extended. The fourth case shown also has $B_0 = 0.44$ T, but has slightly different plasma cross-section (increased elongation), and the computed q_{min} rises to slightly above 2. While the increase in plasma rotation is expected to play a role in RWM stabilization, present theories of energy dissipation by continuum damping in the RWM dispersion relation show a reduction in dissipation, and hence reduced RWM stabilization, as low order rational surfaces are removed

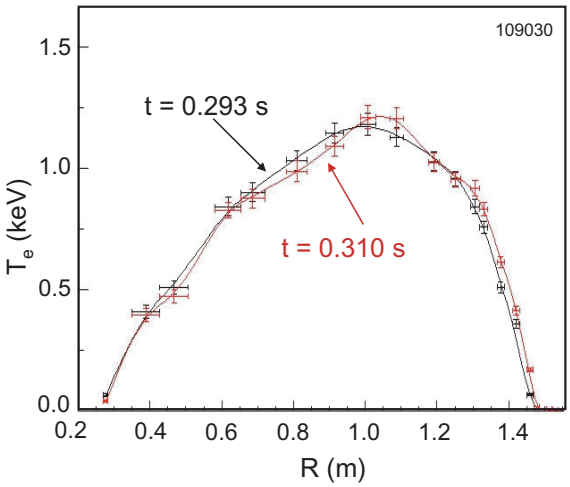

Figure 8. Electron temperature profile evolution during RWM growth.

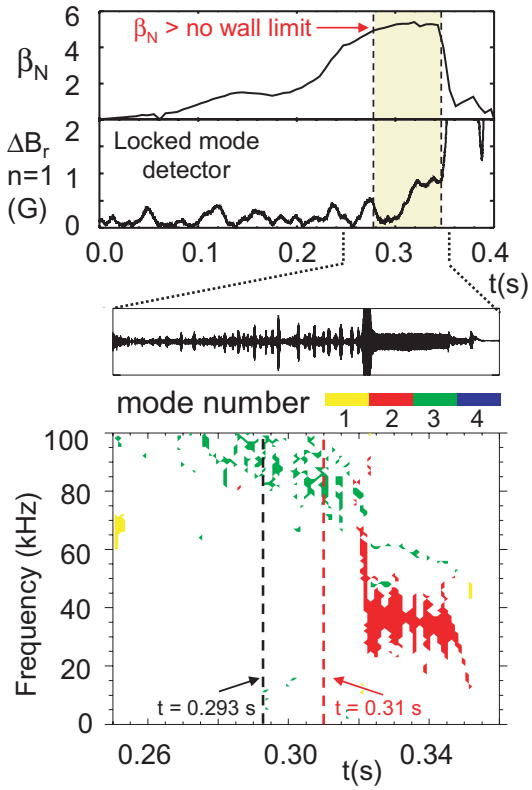

Figure 9. Time evolution of β_N, locked mode signal, and magnetic pickup coil spectra (including toroidal mode number) for plasma exceeding $\beta_{N\,no\text{-}wall}$. The vertical dashed lines indicate the times at which T_e profiles are shown in figure 8. The shaded region of the β_N frame indicates ideal $n = 1$ no-wall instability as computed by DCON.

from the plasma, [13] in contrast to the present observation. Future experiments and analysis will examine this important issue in greater detail.

The time-evolution of both β_N and the $n = 1$ ideal MHD stability criteria with and without a conducting wall is shown in figure 11 for the discharge with the longest duration in figure 10. The maximum NBI power (5 MW) is applied

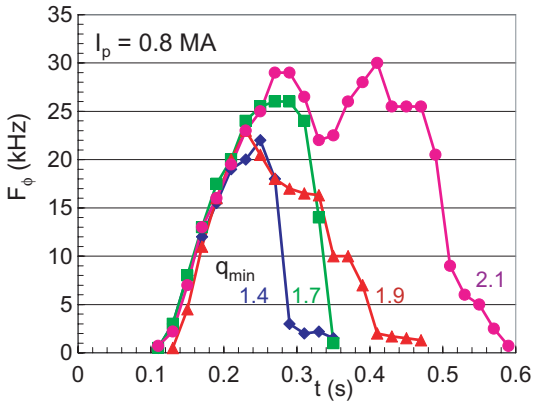

Figure 10. Variation of toroidal rotation damping dynamics as a function of applied toroidal field ($0.34\,\mathrm{T} < B_0 < 0.44\,\mathrm{T}$).

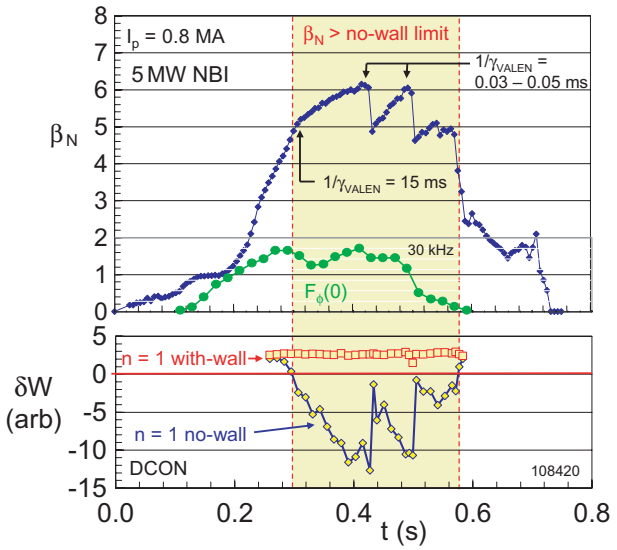

Figure 11. Evolution of β_N, F_ϕ, and ideal no-wall and with-wall stability criteria for a plasma exceeding $\beta_N/\beta_{N\,no\text{-}wall} = 1.3$ and approaching $\beta_{N\,wall}$.

at 0.28 s (as β_N rises through 4). Although an $n = 1$ perturbation is not observed in the LMD, a slowing of the core toroidal rotation at a rate similar to that experienced during RWM destabilization occurs shortly after β_N increases above $\beta_{N\,no\text{-}wall} = 4.7$ at $t = 0.296$ s in this discharge. However, during this initial rotation damping stage, q_{min} rises from a minimum value of 1.2 and reaches 2 by 0.32 s. From this time until after the first beta collapse at 0.43 s, the spectra from magnetic pickup coils do not show an $n = 1$ rotating mode in the plasma. The dominant rotating mode activity has $n = 2$, with weaker $n = 3$ present. As β_N continues to rise in the plasma, the core rotation frequency recovers to the original peak value. The VALEN computed RWM growth time when β_N increases beyond $\beta_{N\,no\text{-}wall}$ is 15 ms. However, as β_N reaches a peak value of over 6.1, VALEN shows a greatly decreased mode growth time of 30 μs, indicating that $\beta_{N\,wall}$ is being approached and passive wall stabilization has become less effective. At this point, a beta collapse occurs in the plasma, reducing β_N to 4.8, at which point the ideal $n = 1$ no-wall stability criterion computed by DCON shows the plasma to be close to marginal stability. This crash,

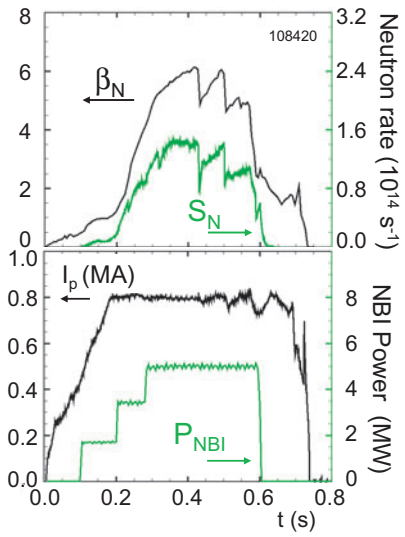

Figure 12. Comparison of neutron and β_N evolution for plasma approaching $\beta_{N\,wall}$. Also shown are the plasma current and programmed NBI pulse for the discharge.

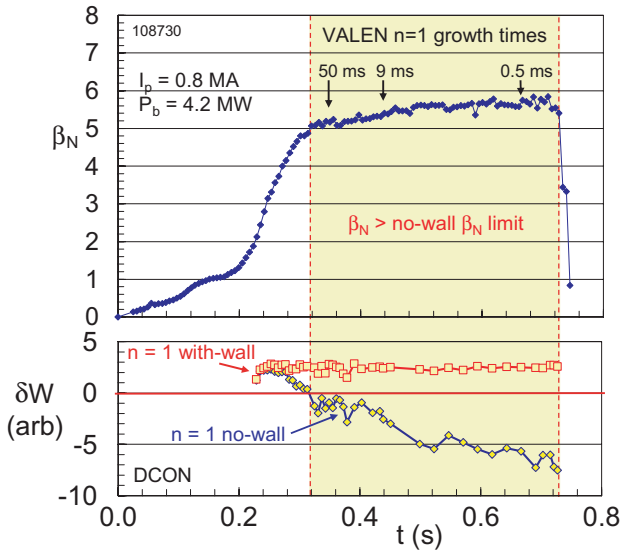

Figure 13. Evolution of β_N and ideal no-wall and with-wall stability criteria for a plasma exceeding $\beta_N/\beta_{N\,no\text{-}wall} > 1$ but remaining below $\beta_N = 6$. Fast β collapses are not observed.

as well as the entire evolution of β_N, correlates closely with the neutron evolution (figure 12). Since the neutrons are produced only in the core of present NSTX plasmas, this correlation indicates that the mode causing the β_N collapse is internal, and the timescale of the collapse suggests an ideal mode growth time. The plasma recovers subsequently and eventually reaches the original peak value of β_N but without an equivalent rise in core rotation frequency. The β_N collapses again back to ideal $n = 1$ no-wall marginal stability, but this time the toroidal rotation decreases rapidly. During this phase, $n = 1$ locked mode activity is evident but is at the noise level of the detector. A relatively slow decrease in toroidal rotation leads eventually to locking of rotating $n = 1$ and $n = 2$ modes and a corresponding large collapse in β_N to below $\beta_{N\,no\text{-}wall}$. Using the relatively large value of $1/\gamma_{VALEN} = 15$ ms for the $n = 1$ RWM perturbation computed with DCON and VALEN when β_N initially exceeds $\beta_{N\,no\text{-}wall}$, a conservative estimate of the plasma duration with $\beta_N/\beta_{N\,no\text{-}wall}$ greater than unity is $18/\gamma_{VALEN}$. The fast, repeated beta collapses shown in figure 11 do not appear to be sawteeth as there is no inversion radius observed, and the collapses are dependent on the magnitude of β_N since similar plasmas have been maintained for longer pulse lengths (duration of greater than $20/\gamma_{VALEN}$) at a slightly lower value of $\beta_N = 5.6$ without fast beta collapses (figure 13). In the discharge shown in figure 11, DCON shows that the plasma is also unstable to the $n = 2$ mode shortly after $n = 1$ instability is determined. Plasma instability to multiple n values was anticipated at high β_N, and future work will investigate the presence of $n = 2$ signatures measured by the LMD.

4. Passive stabilization and active feedback physics design

Growth rates of RWMs interacting with the complex conducting structures in the NSTX device have been computed with the VALEN code [23]. These calculations incorporate the vacuum vessel, centre column, and NSTX conducting plates, designed to provide passive stabilization of the RWM. VALEN uses a finite element representation of thin shell conducting structures in an integral formulation to model arbitrary conducting walls, combined with a circuit representation of stable and unstable plasma modes. A further capability of VALEN is the ability to model arbitrary control coils, magnetic flux sensors, simple power supplies, and control schemes that would be used to connect these items together to provide stabilization of plasma instabilities through active feedback.

The external normal field perturbation of the mode to analyse is computed by DCON from reconstructed experimental equilibria. The external field perturbation is assumed to be non-rotating in the laboratory frame, and rotation effects are not considered in the computation of plasma stability. The model of all passive conductors is combined with the unstable plasma mode, and VALEN is used to perform an eigenvalue analysis to obtain the growth rate of any instabilities. This procedure may be repeated for different equilibria to obtain a scan in β_N. The eigenvalue from VALEN is the growth rate, and the associated eigenvector is the distribution of induced currents in all the conducting structures. Figure 14 illustrates the passive growth rates obtained from such an analysis. For this equilibria scan $\beta_{N\,no\text{-}wall}$ is 5.05 and the VALEN computation of $\beta_{N\,wall}$ is 6.95. The latter value is derived in VALEN by assuming a nearly superconducting passive stabilizing structure. On the right the curve is asymptotic to ideal internal mode growth rates. The growth rate curves, as well as the value of $\beta_{N\,wall}$, depend on the plasma equilibrium parameters. The equilibria used for the scan in figure 14 are derived from an NSTX experimental plasma and have $F_p \sim 2.2$. In good agreement with the experiment, for this class of equilibria, we find $\Delta\beta_N = 2$. Examination of the equivalent surface current generated by the $n = 1$ global mode field perturbation shows that along with the greater mode energy at higher β_N, the computed mode amplitude increases in the divertor region but retains a strong ballooning character with the largest amplitude and long poloidal wavelength in the bad curvature region (figure 15).

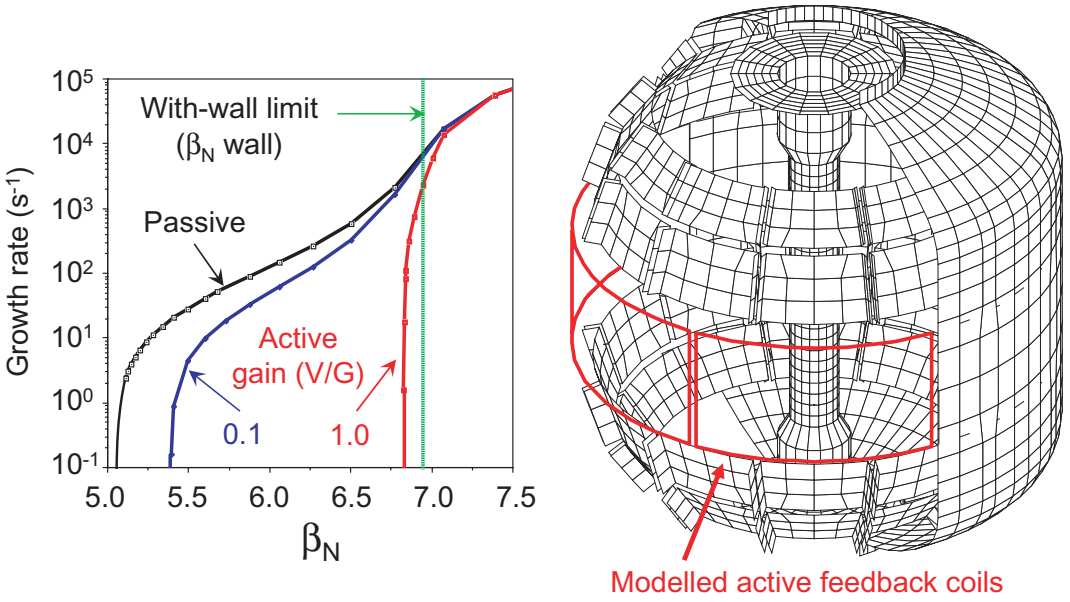

Figure 14. VALEN growth rate versus β_N for the $n = 1$ mode considering passive and active feedback systems with gains of 0.1 and 1.0 V G^{-1}. The active feedback system has control coils inside the vacuum vessel.

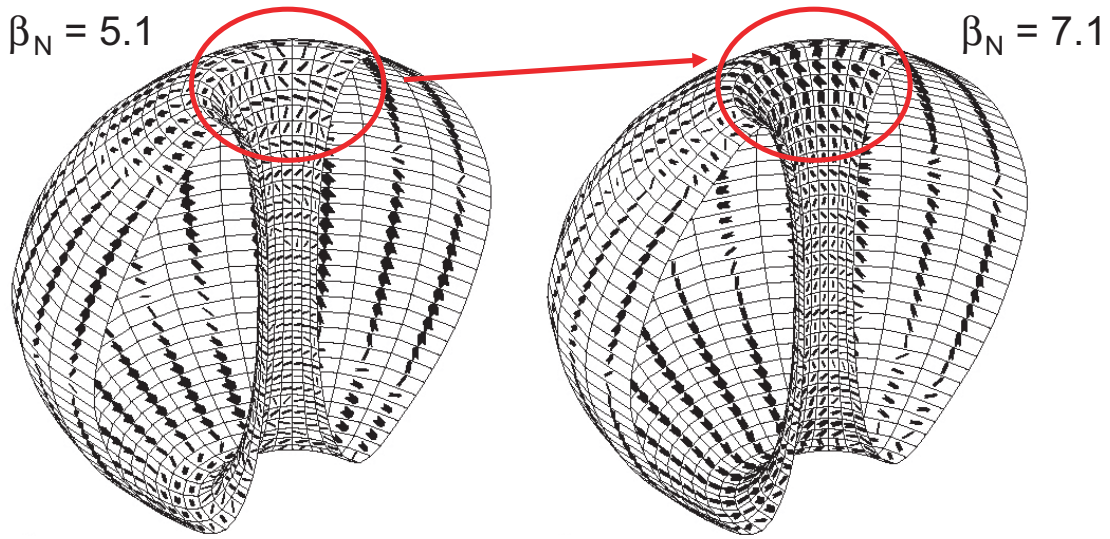

Figure 15. VALEN computed currents from DCON ideal $n = 1$ external unstable eigenmode. Mode strength increases closer to the divertor region (further from NSTX conducting plates) in high β_N plasmas.

An active feedback system can be used to stabilize the RWM in a plasma with low toroidal rotation, as is expected in a reactor. Previous calculations using VALEN for the DIII-D device indicate that the most effective systems have control coils positioned as close as possible to the plasma and with minimal coupling to major conducting structures. A mode control scheme typically uses a global array of magnetic sensors placed inside the vacuum vessel as close as possible to the plasma and oriented to sample the poloidal field of an instability while being orthogonal to the field produced by the closest control coils. The structure of the instability may then be identified, and then feedback logic determines the currents or voltages applied to the control coils.

A near optimal active feedback system designed to suppress the $n = 1$ instability in NSTX has been studied computationally. In this case, the modelled sensors are positioned inside the vacuum vessel on the plasma midplane and measure the poloidal field of the instability. Control coils were placed inside the vacuum vessel. Six equal sized picture frame coils, which produce local radial fields, cover the midplane circumference of NSTX and are connected 'anti-pairwise' (control coils diametrically opposite each other are in a series circuit, and their radial fields are in the same direction). The sensors have a single turn and an area of 1·e−04 m^2. The mode perturbed flux measured by the sensors is multiplied by a constant gain to determine the voltage applied to the control coils. A unity gain signifies that a poloidal perturbation averaged over the sensor loop area of 1 G calls for the application of 1 V to a control coil. Figure 14 illustrates the performance of this system. At a gain of 0.1, the plasma is stable for beta normal less than 5.39. A further improvement in performance may be obtained by increasing the gain up

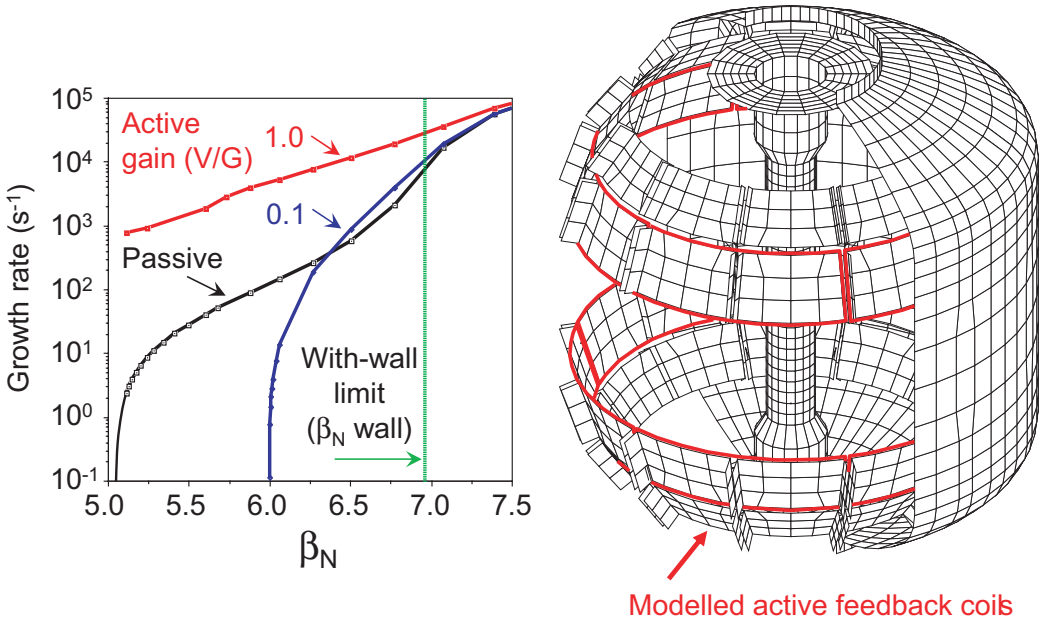

Figure 16. VALEN growth rate versus β_N for the $n = 1$ mode considering passive and active feedback systems with gains of 0.1 and 1.0 V G^{-1}. The active feedback system has control coils that encircle the primary passive plates of the device.

to about 1.0, where the plasma is stable for beta normal less than 6.83. The active feedback system shows no further improvement for additional increases in gain. Since the plasma is stable with $\beta_N < \beta_{N\,no\text{-}wall}$, proximity to the with-wall beta limit is typically quantified as $(\beta_N - \beta_{N\,no\text{-}wall})/(\Delta\beta_N)$. Using this ratio, this system can stabilize the mode in plasmas with β_N up to 94% of the ideal wall limit.

Alternatives to the 'near optimal' active feedback design were considered. The first keeps the poloidal field sensors interior to the vacuum vessel but moves the control coils outside. This system reaches a maximum stabilized $(\beta_N - \beta_{N\,no\text{-}wall})/(\Delta\beta_N) = 72\%$, a decrease of 22% from the near optimal design. The final configuration considered moved the control coils of the midplane and placed them in the gaps between the primary passive plates (figure 16). The six coils on the midplane are replaced by six coils among the upper primary passive plates and six coils among the lower primary passive plates. The coils no longer produce a pure radial field because they have a tilt that matches the primary passive plates. This system reaches a maximum stable $(\beta_N - \beta_{N\,no\text{-}wall})/(\Delta\beta_N)$ of only 50%. At a gain of 1 V G^{-1}, this active system is overdriven and underperforms the passive stabilization system. The reduced system performance is due to the coupling of the control coils to the passive plates they surround.

5. Summary and conclusions

High β_N plasmas have been created in NSTX that are passively stabilized to global MHD instabilities by a conducting structure. As was theoretically anticipated, low aspect ratio plasmas enable stable operation experimentally at a high β_N/l_i, presently reaching 9.5. In addition, empirical stability limits where β_N/l_i is a constant encountered in advanced tokamak plasmas do not appear to apply in the wall stabilized regime of the ST. An increase in maximum achieved β_N at decreasing pressure peaking is observed. Creation of an increased region of passive stability ($\Delta\beta_N = 2$) and increased discharge longevity has been achieved by reduction of the $n = 1$ static error field, H-mode operation, and an increase in applied toroidal field from 0.3 to 0.4 T or greater. Close proximity to passive conducting structure is not required at a high β_N due to the long outboard poloidal wavelength and therefore strong coupling of low-n global MHD modes that occurs in ST geometry. The observed β_N limit is insensitive to the magnitude of the outer gap at a high β_N. RWMs are observed, now more frequently accompanied by rotating modes. RWM plasmas exceeding the ideal no-wall β_N limit can have plasma toroidal rotation damping rates more than five times greater than in plasmas with β_N below the ideal no-wall limit and with rotating modes alone. The rotation damping during the RWM is global, rather than the local and diffusive character of the rotation damping observed when only rotating modes are present. The global mode damping agrees qualitatively with the non-resonant theory of rotation damping by neoclassical toroidal viscosity in the helically perturbed field of the instability. Toroidal rotation damping at $\beta_N > \beta_{N\,no\text{-}wall}$ can presently be curtailed by operation at an increased toroidal field such that the computed equilibrium $q_{min} > 2$, and a β_N up to 6 can be maintained for pulse lengths reaching a current relaxation time without the discharge suffering beta-limiting instability. Fast beta collapses caused by internal modes are observed as β_N exceeds 6 and the ideal no-wall beta limit is approached.

While passive stabilization can be effective with sufficient plasma rotation, maintenance of such a condition may be difficult at higher β_N in NSTX and in future devices. Therefore, the physics design of an active feedback coil system was performed, anticipating installation of such a system for future experimental studies. A system with a relatively simple set of control coils positioned at the midplane of the device is

computed to be sufficient to sustain operation at a β_N of 94% of the ideal with-wall limit. The long outboard poloidal wavelength of low-n global modes at a high β_N in the ST eliminates the need for a complex control coil geometry to couple optimally to the mode, yielding a simple, yet high performance stabilization system.

Acknowledgments

The first author (S.A.S.) would like to acknowledge important discussions with Dr Riccardo Betti regarding RWM dissipation mechanisms and Drs C. Hegna, J.D. Callen, and K. Shaing regarding rotation damping of viscous plasma in a perturbed helical field. This research was supported by the US Department of Energy under contracts DE-FG02-99ER54524 and DE-AC02-76CH03073.

References

[1] Peng Y.-K.M. and Strickler D.J. 1986 *Nucl. Fusion.* **26** 769
[2] Stambaugh R.D., Chan V.S., Miller R.L. and Schaffer M.J. 1998 *Fusion Technol.* **33** 1
[3] Ono M. *et al* 2000 *Nucl. Fusion* **40** 557
[4] Garofalo A.M. *et al* 2001 *Nucl. Fusion* **41** 1171
[5] Menard J.E. *et al* 2003 *Nucl. Fusion* **43** 330
[6] Glasser A.H. and Chance M.S. 1997 *Bull. Am. Phys. Soc.* **42** 1848
[7] Sabbagh S.A. *et al* 2002 *Phys. Plasmas* **9** 2085
[8] Howl W. *et al* 1992 *Phys. Fluids* B **4** 1724
[9] Maingi R. *et al* 2002 *Phys. Rev. Lett.* **88** 035003
[10] Lao L.L. *et al* 1985 *Nucl. Fusion* **25** 1611
Sabbagh S.A., Kaye S.M., Menard J.E. *et al* 2001 *Nucl. Fusion* **41** 1601
[11] Bondeson A. and Ward D.J. 1994 *Phys. Rev. Lett.* **72** 2709
[12] La Haye R.J., Hyatt A.W. and Scoville J.T. 1992 *Nucl. Fusion* **32** 2119
[13] Betti R. 1998 *Phys. Plasmas* **5** 3615
[14] Strait E.J. *et al* 1994 *Phys. Rev. Lett.* **74** 2483
[15] Garofalo A.M. *et al* 2000 *Nucl. Fusion* **40** 1491
[16] Betti R. and Freidberg J.P. 1995 *Phys. Rev. Lett.* **74** 2949
[17] Lazzaro E. *et al* 2002 *Phys. Plasmas* **9** 3906
[18] LaHaye R. *et al* 2002 *Phys. Plasmas* **9** 2051
[19] Fitzpatrick R. 1993 *Nucl. Fusion* **33** 1049
[20] Smolyakov A.I. *et al* 1995 *Phys. Plasmas* **2** 1581
[21] Shaing K.C. *et al* 1986 *Phys. Fluids* **29** 521
[22] Synakowski E. *et al* 2003 *Nucl. Fusion* **43** 1653
[23] Bialek J., Boozer A.H., Mauel M.E. and Navratil G.A. 2001 *Phys. Plasmas* **8** 2170